# *Supplementary information*

## MOFs-Derived N,S Co-doped Carbon Matrix Encapsulated Cu$_2$S Nanoparticles as High-Performance Lithium-Ion Battery Anodes: A Joint Theoretical and Experimental Study

Tianlin Li[b#], Danyang Zhao[a#]*, Meiyu Shi[a], Tongde Wang[c], Qing Yin[a], Yongzhi Li[a], Jiqiu Qi[a], Fuxiang Wei[a], Yanwei Sui[a]*

[a]Jiangsu Province Engineering Laboratory of High-Efficient Energy Storage Technology and Equipment, School of Materials Science and Physics, China University of Mining and Technology, Xuzhou 221116, P R China

[b]School of Chemical Engineering and Technology, China University of Mining and Technology, Xuzhou 221116, P R China

[c]Shanghai Key Laboratory of Special Artificial Microstructure Materials and Technology, School of Physics Science and Engineering, Tongji University, Shanghai 200092, China

*Corresponding authors E-mails: zhao_dy@cumt.edu.cn (Danyang Zhao)

wyds123456@outlook.com (Yanwei Sui)

[#] Tianlin Li and Danyang Zhao contribute equally to this work.

# 1. Experimental

## 1.1 Materials.

Copper nitrate hydrate ($Cu(NO_3)_2 \cdot 3H_2O$), benze-1,3,5-tricarboxylate, polyvinyl pyrrolidone (PVP), urea, thioacetamide (TAA), acetylene black, melamine, polyvinylidene difluoride (PVDF), N-methylpyrrolidone (NMP), ethanol (AR, 99.5%) are ordered from Aladdin Reagents (Shanghai) Co., Ltd. All chemicals are used directly without any further treatment.

## 1.2 Synthesis of N-Cu-BTC and Cu-BTC precursors.

6 mmol $Cu(NO_3)_2 \cdot 3H_2O$ is ultrasonically dissolved in 30 mL deionized water (solution A), 0.65 g 1,3,5-benzentricarboxyllic acid, melamine and 0.5g PVP are ultrasonically dissolved in 30 mL anhydrous ethanol (solution B). After stirring for 30 min, the solution A is quickly poured into solution B, and the mixed solution is continuously stirred for 1h to form a uniform blue solution. The above solution is transferred to a 100 mL Teflon-lined autoclave and kept at 120 ℃ for 12 h. After cooling to room temperature, the blue precipitate is separated by centrifugation and washed with anhydrous ethanol and deionized water. The final Cu-BTC (BTC= benze-1,3,5-tricarboxylate) precursor is vacuum dried at 70 ℃ for 12 h.

For comparison, Cu-BTC precursor is obtained under the same conditions without melamine in solution B.

## 1.3 Synthesis of Cu$_2$S@NSC and Cu$_2$S@SC.

A certain amount of TAA and prepared N-Cu-BTC precursor with a mass ration of 10:1 is placed into two quartz boats respectively, and TAA is arranged upstream. N-Cu-BTC powders are vulcanized at 600 ℃ for 3h with a heating rate of 3℃ min$^{-1}$ in flowing Ar atmosphere. After naturally cooling down to room temperature, the black product is collected and coded as Cu$_2$S@NSC.

The Cu$_2$S@SC is synthesized by the same process with the precursor of Cu-BTC. To obtain monophasic Cu$_2$S sample, the Cu-BTC blue powders are calcined at 600 ℃ for 2 h in N$_2$ atmosphere and transform into CuO. After the same sulfuration treatment, Cu$_2$S powders can be obtained.

## 1.4 Materials characterization.

Raman scattering spectra is recorded with a Renishaw System 2000 spectrometer, and the wavelength of the laser is 532 nm. The crystal structure and phase composition are analyzed by X-ray diffraction (XRD, Bruker D8) with Cu Kα radiation (λ=0.1518 nm), between 10 and 80°. X-ray photoelectron spectroscopy (XPS, Thermo ESCALAB 250XI) is used to determine the chemical state of samples. The TG analysis is performed using a TA analyzer.

## 1.5 Electrochemical measurement.

Electrodes are prepared by mixing active materials, acetylene black, and PVDF with a mass ratio of 8:1:1 in NMP. The uniformly ground slurry is coated with designated thickness onto copper foil (for anode), drying at 100 °C for 12 h under vacuum. Assembling LIBs (CR2032) with Li foil as counter electrode to test the electrochemical properties of $Cu_2S$, $Cu_2S@SC$ and $Cu_2S@NSC$ anodes. The electrolyte is composed of 1M $LiPF_6$ in ethylene carbonate/dimethyl carbonate. The galvanostatic charge/discharge (GCD) are carried out at 0.01-3.0 V, tested by Land cell measurement system (Wuhan Land Electronics Co., Ltd.). Cyclic voltammetry (CV) test is carried out at RST5080F electrochemical workstation.

## 1.6 DFT calculation details.

The first-principles calculations are implemented in the vienna ab-initio simulation package (VASP) software.[1] Plane wave generator project augmented wave (PAW) pseudopotential is used to describe the interaction between ions and electrons, and the interaction of electron exchange is handled by Perdew-Burke-Ernzerhof (PBE) functional of generalized gradient approximation (GGA). [2,3] The cut-off energy is set to 487, 520 and 650 eV, the force and energy convergence standards of each atom are 0.05 eV $Å^{-1}$ and $10^{-5}$ eV, respectively. To avoid the interactions between the upper and lower atomic layers, the vacuum layer is set to 20 Å.

Three models of $Cu_2S$, $Cu_2S@SC$ and $Cu_2S@NSC$ are constructed. K-point network spaces of 3×3×1, 4×4×1 and 3×4×1 are respectively used to optimize the model structure. The construction is completed with the aid of the vaspkit module in the software. The calculation of elemental atoms energy is done in a 20×20×20 $Å^3$

unit cell. In addition, since the copper in the model is a transition metal element, the system contains strongly related d-orbital and f-orbital electrons, and their strong interaction will cause non-local problems of electrons, leading to underestimation of the band gap. Therefore, we use the DFT+U energy functional to ensure the accuracy of the calculation.[4]

Surface energy can be established as a vital index to measure surface stability, which could be expressed by **Eq. S1**:[5]

$$E_{surf} = \frac{1}{2A}(E_{slab} - nE_{bulk})$$

(S1)

Where $n$ is the number of atoms contained in slab; $E_{slab}$ is the total energy of the selected slab model; $E_{bulk}$ is the energy of each proto-cell; $A$ is the surface area of cystal cell.

The surface work function is the minimum energy required for electrons to move from the interior of a solid to the surface, which can be determined by **Eq. S2**:[6]

$$E_{wf} = E_{vacuum} - E_{fermi}$$

(S2)

where $E_{vacuum}$ is the electrostatic potential energy at the vacuum away from the surface; $E_{fermi}$ is the electrostatic potential energy at the Fermi level.

To evaluate the Li/Na/K adsorption capacity of different materials, **Eq. S3** is used to calculate the adsorption energy ($E_{ad}$):[7]

$$E_{ad} = E_{structure + atom} - E_{structure}$$

(S3)

where $E_{Structure + atom}$ and $E_{Structure}$ are respectively the total energy of the metal atoms adsorbed on the $Cu_2S$ surface and the energy of the $Cu_2S$ in the same cell.

The change in the diffusion coefficient of metal ions with temperature can be calculated using the Arrhenius **Eq. S4**:[8]

$$D = D_0 \, exp\left(-\frac{\Delta E_b}{KT}\right)$$

(S4)

where $D_0$, $\Delta E_b$, $K$ and $T$ are the pre-exponential factor, activation energy (diffusion barrier), Boltzmann's constant and the absolute temperature.
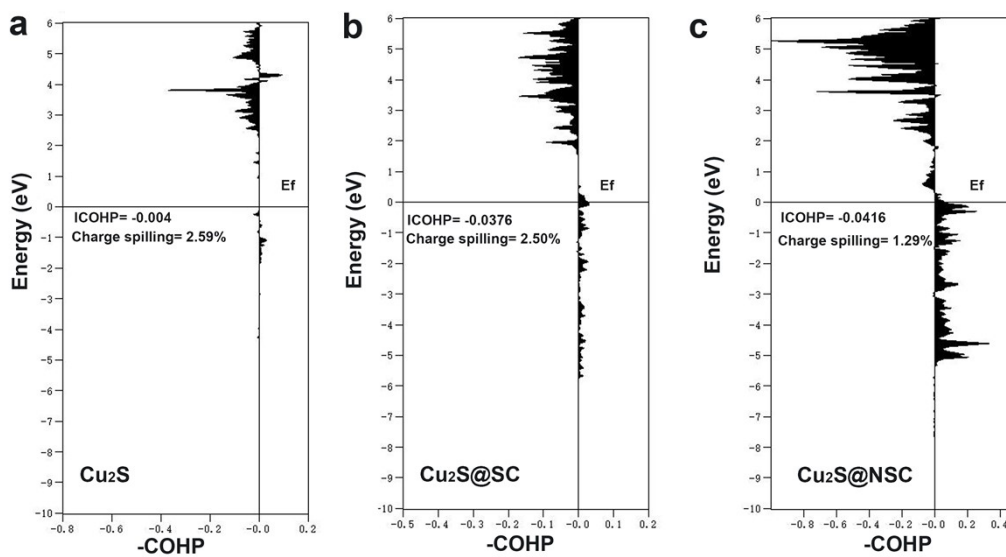
# 2. Figures



**Fig. S1** COHP of Li-S for (a) $Cu_2S$, (b) $Cu_2S@SC$ and (c) $Cu_2S@NSC$.
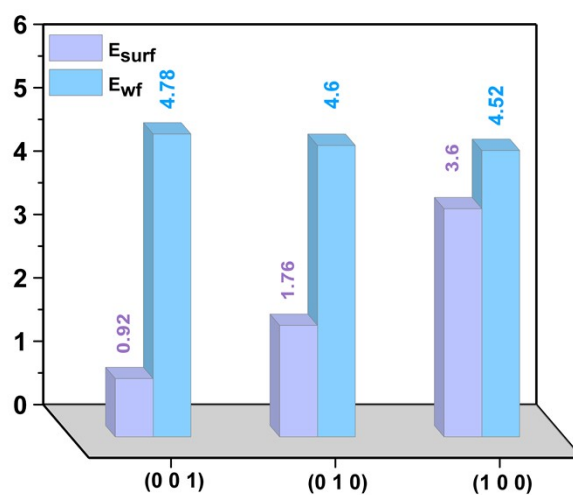


**Fig. S2** Surface energy and work function of $Cu_2S$ (001), $Cu_2S$ (010) and $Cu_2S$ (100).
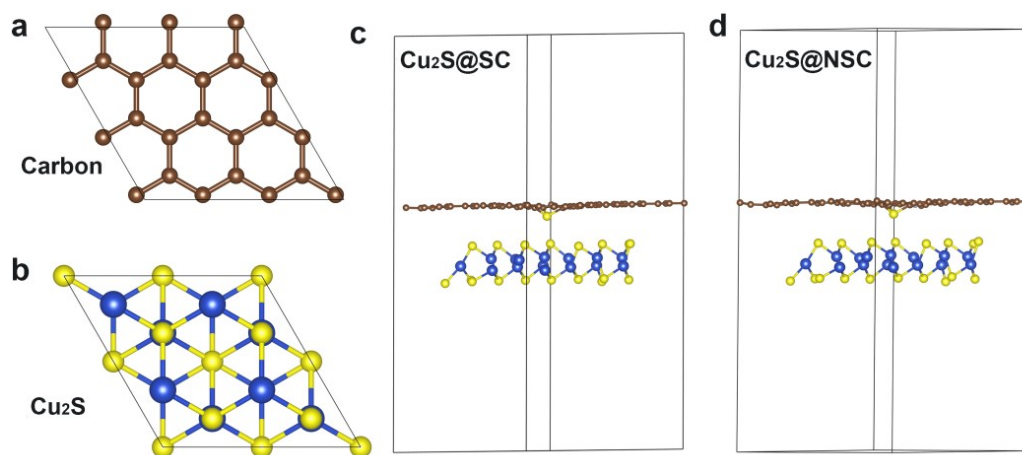
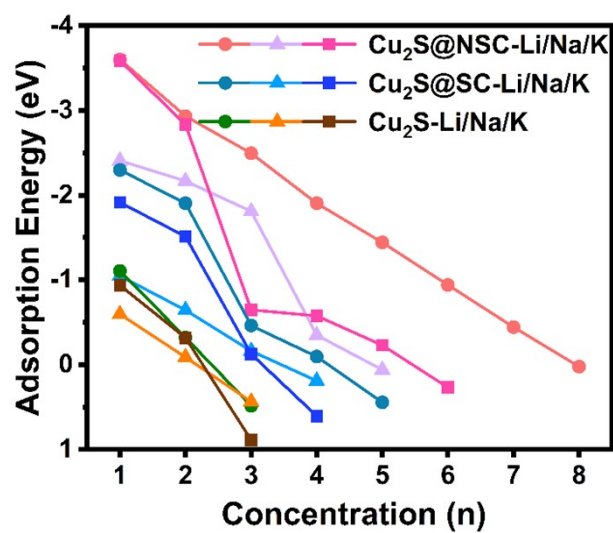**Fig. S3** Structure of (a) carbon, (b) $Cu_2S$, (c) $Cu_2S@SC$ and (d) $Cu_2S@NSC$.



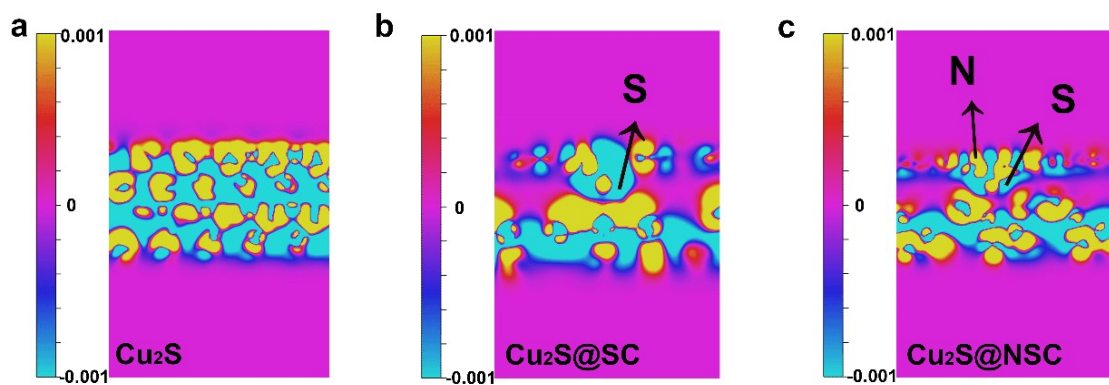**Fig. S4** Adsorption energy with increase of the number of alkali metal atoms.

**Fig. S5** Charge distribution on (a) $Cu_2S$, (b) $Cu_2S@SC$ and (c)$Cu_2S@NSC$.



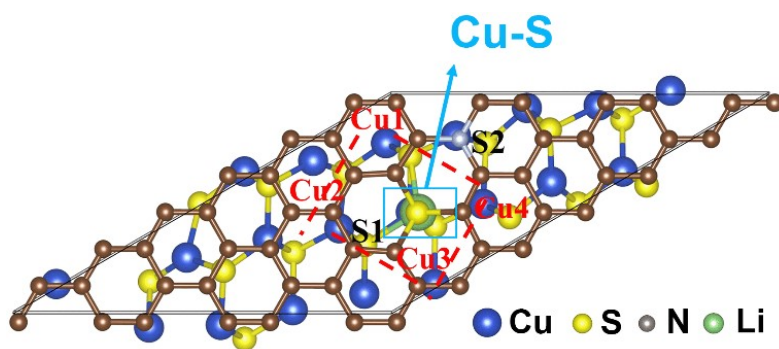**Fig. S6** Li adsorption sites on $Cu_2S@NSC$.
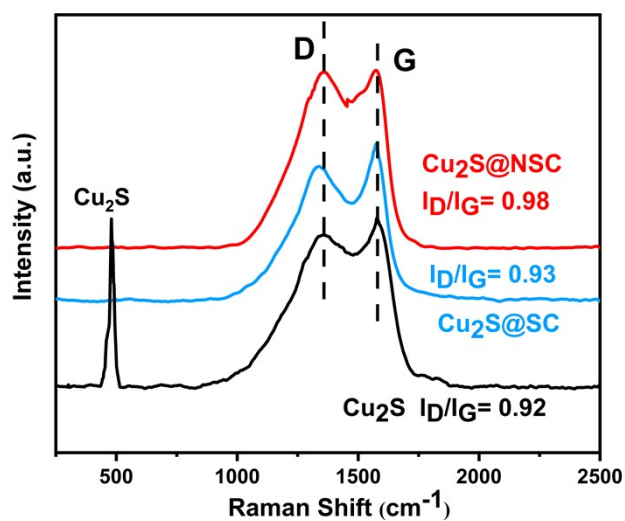


**Fig. S7** Raman spectra of $Cu_2S$, $Cu_2S@SC$ and $Cu_2S@NSC$.

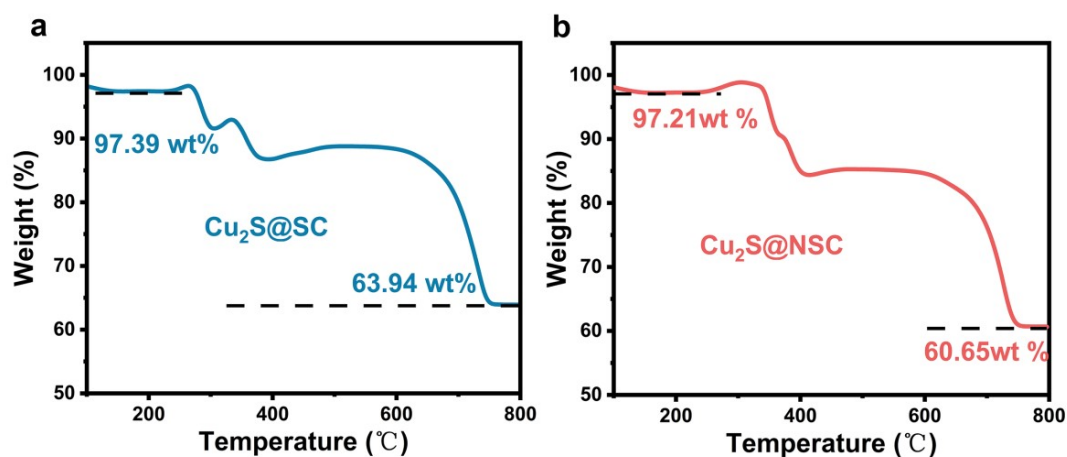**Fig. S8** TG curves of (a) $Cu_2S@SC$ and (b) $Cu_2S@NSC$.

In air conditions, $Cu_2S$ experiences different oxidation and decomposition reactions. The initial mass drop at around 100 °C arises from water evaporation. Subsequently, the weight loss is own to the decomposition and oxidation of $Cu_2S$ and carbon in air atmosphere. Obviously, the carbon could be totally decomposed at around 600°C, and $Cu_2S$ can be completely converted to $Cu_2O$ at around 800°C. Based on above analysis, one can calculate the amount of $Cu_2S$ in $Cu_2S@SC$ and $Cu_2S@NSC$ composites using the weight percent of $Cu_2O$ at 800°C. The calculated weight percentage of carbon in $Cu_2S@SC$ and $Cu_2S@NSC$ composites is 26.67% and 29.75 %.
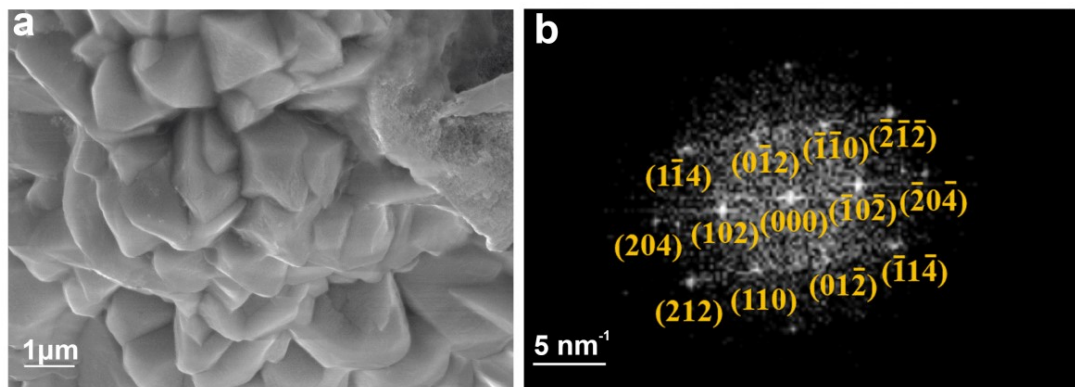
**Fig. S9** (a) SEM image and (b) SAED pattern of Cu$_2$S.



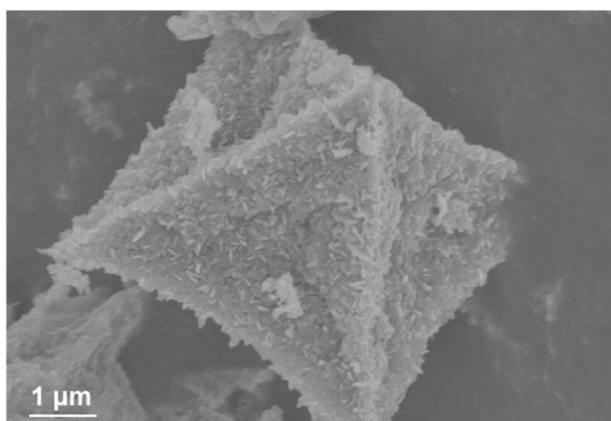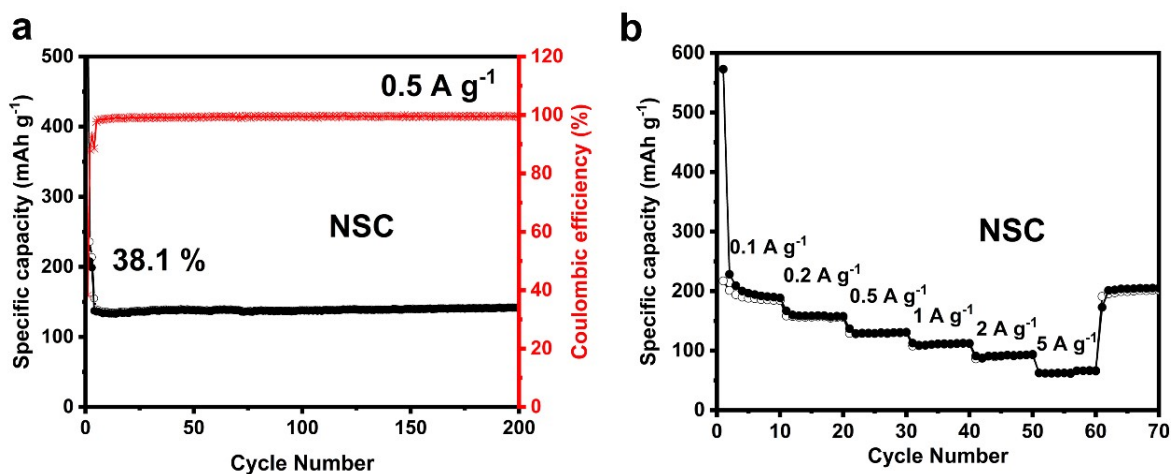**Fig. S10** SEM image of Cu$_2$S@SC.



**Fig. S11** (a) Cycle performance at 0.5 A g$^{-1}$, (b) rate capability at current densities ranging from 0.1 to 5 A g$^{-1}$ of NSC electrode.
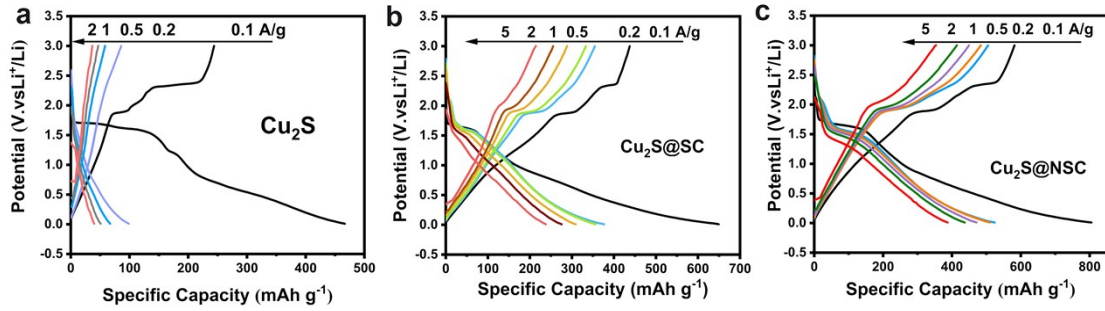
**Fig. S12** (a) Rate capabilities at different current densities (a) Cu₂S, (b) Cu₂S@SC and Cu₂S@NSC electrodes.



**Fig. S13** (a) CV curves at 0.1 to 1.0 mV s⁻¹, (b) b values of redox peaks, (c) pseudocapacitance contribution at 1.0 mV s⁻¹ and (d) different scan rate of Cu₂S electrode.

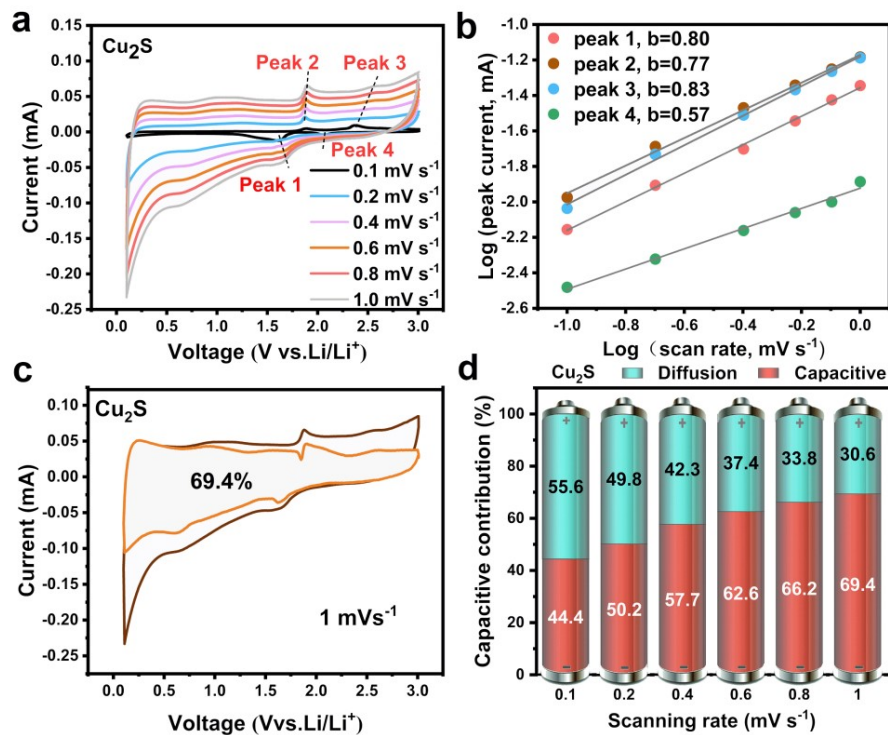**Fig. S14** (a) CV curves at 0.1 to 1.0 mV s$^{-1}$, (b) b values of redox peaks, (c) pseudocapacitance contribution at 1.0 mV s$^{-1}$ and (d) different scan rate of Cu$_2$S@SC electrode.
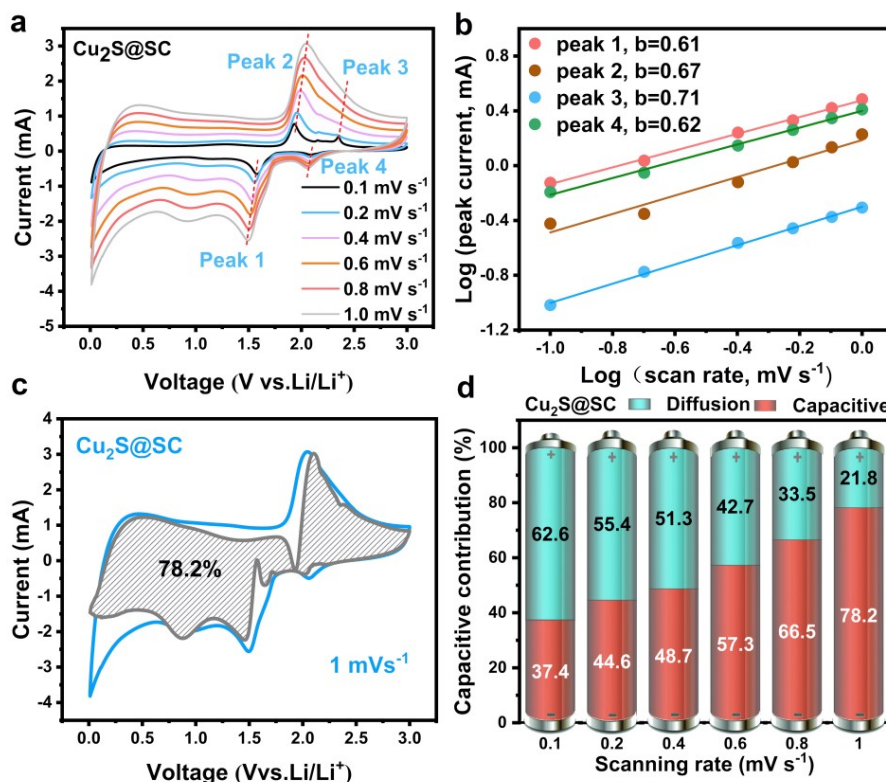


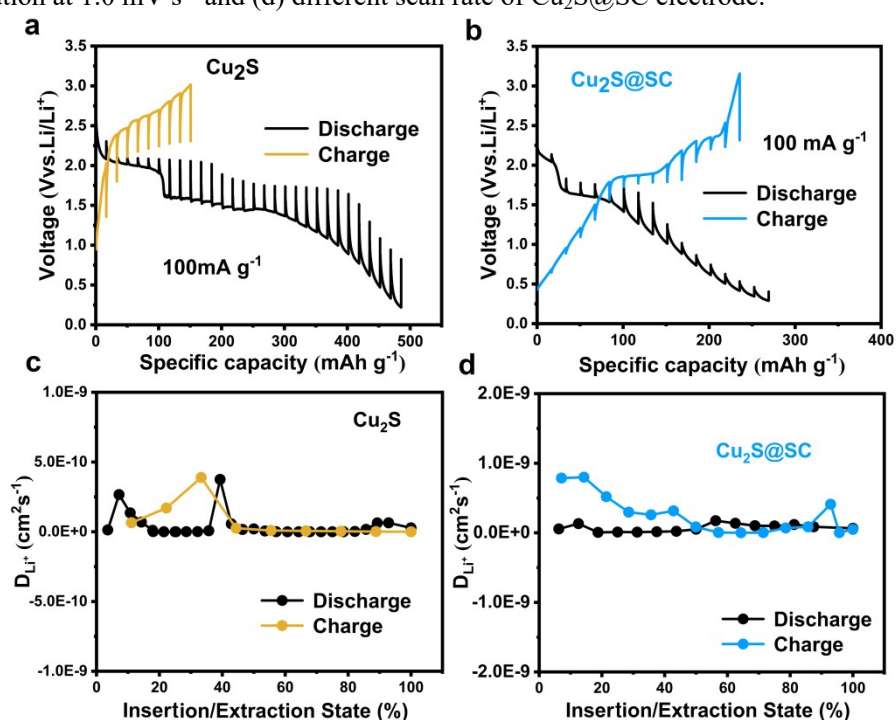**Fig. S15** (a-b) GITT curve of the Cu$_2$S and Cu$_2$S@SC electrodes. (c-d) Calculate the Li$^+$ diffusion system of the Cu$_2$S and Cu$_2$S@SC electrodes.

The Li$^+$ ion diffusion coefficients for different charge/discharge states are

obtained according to the **Eq. S5**:

$$D_{Li^+} = \frac{4}{\pi r}\left(\frac{m_B V_m}{M_B A}\right)^2 \left(\frac{\Delta E_S}{\Delta E_\tau}\right)^2 \left(\tau \ll L^2/D_{Li^+}\right)$$

(S5)

Where $M_B$ and $m_B$ respectively denotes the molecular weight and the mass of the active substance; $V_m$ is the molar volume; $A$ is the surface area of the electrode; $L$ expresses the thickness of the electrode; $\Delta E_S$ and $\Delta E_\tau$ are respectively depict the voltage change after the current flux and the open state and the voltage change during the constant current pulse process.
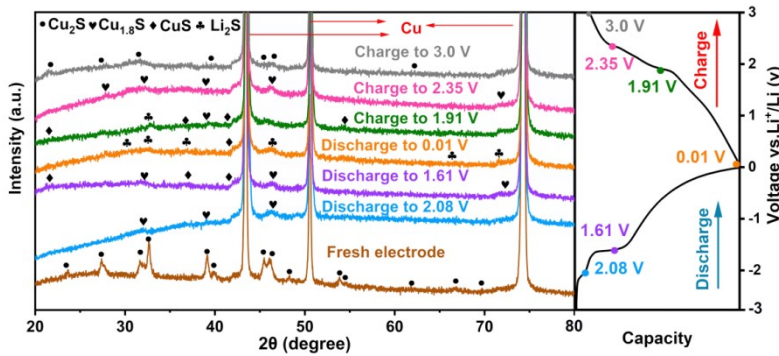


Fig. S16 Ex-situ XRD patterns of Cu$_2$S@NSC electrode during the first cycle.

## 3. Tables

Table S1. The BFDH calculation results.

| (h k l) | Distance | Total facet area | Total facet area percentage (%) |
|---------|----------|------------------|--------------------------------|
| (0 0 1) | 8.89 | 2508.03 | 29.23 |
| (0 0 -1) | 8.89 | 2508.03 | 29.23 |
| (1 0 0) | 25.04 | 891.33 | 10.39 |
| (-1 0 0) | 25.04 | 891.33 | 10.39 |
| (0 1 0) | 25.04 | 891.33 | 10.39 |
| (0 -1 0) | 25.04 | 891.33 | 10.39 |

Table S2. Electrode resistances obtained from the equivalent circuit fitting.

| | $V_{OC}$ (V) | $R_e$ (Ω) | $R_{ct}$ (Ω) | Warburg factor σ | $D_{Li^+}$ (S cm$^{-1}$) |
|---|---|---|---|---|---|
| Cu$_2$S | 2.41 | 0.96 | 160.70 | 443.19 | $4.76\times10^{-9}$ |
| Cu$_2$S@SC | 2.90 | 1.28 | 44.15 | 38.17 | $6.41\times10^{-7}$ |
| Cu$_2$S@NSC | 2.78 | 1.42 | 23.56 | 23.41 | $1.76\times10^{-6}$ |

The diffusion rate of lithium ion can be calculated by using the low-frequency data according to the following formula:[11,12]

$$D_{Li^+} = \frac{R^2T^2}{2A^2n^2F^4C_{Li}^2\sigma^2}$$

(S6)

Where $D_{Li^+}$ is the Li$^+$ ions diffusion efficiency, $R$ is the ideal gas constant, $T$ is the absolute temperature (298.15 K), $A$ is the surface area of the electrode ($\pi\times0.7^2$), $n$ is the number of transferred electrons per Cu$_2$S molecule during oxidization process (n=4), $F$ is the Faraday constant (96485 C), $C$ is the Li$^+$ ions concentration ($1.0\times10^{-6}$ mol cm$^{-3}$), $\sigma$ is the Warburg factor which can be obtain from **Eq. S6**.

**Table S3** Comparison on discharge reversible capacity and cycling performance between our work and resent Cu$_2$S-based publications.

| Materials | Current density (mA g$^{-1}$) | Cycle numbers | Reversible capacity (mAh g$^{-1}$) | Reference |
|---|---|---|---|---|
| CNT-Cu$_2$S | 100 | 200 | 260 | [10] |
| Cu$_2$S/MoS$_2$/rGO | 500 | 200 | 607. | [11] |
| Cu$_2$S/C | 100 | 100 | 300 | [12] |
| Cu$_2$S/C | 100 | 200 | 523 | [13] |
| Cu$_2$S@NC | 500 | 350 | 350 | [14] |
| Cu$_2$S | 100 | 50 | 242.8 | [15] |
| Cu$_2$S/C | 200 | 300 | 270 | [16] |
| Cu$_2$S/rGO | 100 | 200 | 600 | [17] |
| Cu$_2$S@NSC | 500/1000 | 200/1000 | 662.6/512.7 | This work |

## Supplementary reference

1. V. Wang, N. Xu, J. C. Liu, G. Tang and W. T. Geng, *Comput. Phys. Commun.*, 2021, **267**, 108033.
2. A. Urban, D. H. Seo and G. Ceder, *npj Comput. Mater*, 2016, **2**, 16002.
3. D. Datta, J. Li and V. B. Shenoy, *ACS Appl. Mater. Interfaces*, 2014, **6**, 1788-1795.
4. F. Marsusi, N. D. Drummond and M. J. Verstraete, *Carbon*, 2019, **144**, 615-627.
5. Y. Jiang, G. Zhang, T. Liu, Z. Yang, Y. Xu, R. Lin and X. Wang, *J. Hazard. Mater.*, 2022, **430**, 128434.
6. A. Etxebarria, S. L. Koch, O. Bondarchuk, S. Passerini, G. Teobaldi and M. Á. Muñoz-Márquez, *Adv. Energy Mater.*, 2020, **10**, 2000520.
7. Q. Li, R. García-Muelas and N. López, *Nat Commun*, 2018, **9**, 526.
8. K. Liu, J. Wang, H. Zheng, X. Sun, Z. Yang, J. Man, X. Wang and J. Sun，*J. Mater. Sci. Technol.*, 2022, **104**, 88-97.
9. Q. Peng, S. Zhang, H. Yang, B. Sheng, R. Xu, Q. Wang and Y. Yu, *ACS Nano*, 2020, **14**, 6024-

    6033.

10. X. Meng, S. C. Riha, J. A. Libera, Q. Wu, H.-H. Wang, A. B. F. Martinson and J. W. Elam, *J. Power Sources*, 2015, **280**, 621-629.

11. Y. Rao, K. Zhu, P. Liang, J. Zhang, H. Zheng, J. Wang, J. Liu, K. Yan and N. Bao, *CrystEngComm*, 2022, **24**, 4698-4704.

12. Y. Rao, K. Zhu, P. Liang, J. Zhang, H. Zheng, J. Wang, J. Liu, K. Yan and N. Bao, *Int. J. Hydrogen Energy*, 2015, **40**, 670-674.

13. G. Tian, C. Huang, X. Luo, Z. Zhao, Y. Peng, Y. Gao, N. Tang and S. Dsoke, *Chem. Eur. J.*, 2021, **27**, 13774-13782.

14. J. Han and J. Ren, *J Mater Sci*, 2021, **56**, 19119-19127.

15. C. Shi, X. Li, X. He and J. Zhao, *Electrochim. Acta.*, 2015, **174**, 1079-1087.

16. F. Han, W. C. Li, D. Li and A. H. Lu, *CHEMELECTROCHEM*, 2014, **1**, 733-740.

17. X. Zhang, L. Duan, X. Zhang, X. Li and W. Lü, *J. Alloys Compd.*, 2020, **816**, 152539.